arXiv:1212.3861v1 [cond-mat.dis-nn] 17 Dec 2012

Quantitative prediction of effective toughness at random heterogeneous interfaces

Sylvain Patinet,[1, 2] Damien Vandembroucq,[1, 3] and Stéphane Roux[4]
[1]*Laboratoire PMMH, ESPCI/CNRS-UMR 7636/Univ. Paris 6 UPMC/Univ. Paris 7 Diderot*
10 rue Vauquelin, 75231 Paris cedex 05, France
[2]*Dep. of Materials Science and Engineering, Johns Hopkins University, Baltimore, Maryland 21218, USA*
[3]*The Niels Bohr Institut, Blegdamsvej 17, DK-2100 Copenhagen, Denmark*
[4]*LMT-Cachan, ENS de Cachan/CNRS-UMR 8535/Université Paris 6/PRES UniverSud Paris*
61 Avenue du Président Wilson, 94235 Cachan cedex, France
(Dated: December 18, 2012)

The propagation of an adhesive crack through an anisotropic heterogeneous interface is considered. Tuning the local toughness distribution function and spatial correlation is numerically shown to induce a transition between weak to strong pinning conditions. While the macroscopic effective toughness is given by the mean local toughness in case of weak pinning, a systematic toughness enhancement is observed for strong pinning (the critical point of the depinning transition). A self-consistent approximation is shown to account very accurately for this evolution, *without any free parameter*.

Introduction - While the intimate link between surface energy of a material, and the resistance to crack propagation, or toughness, has been elucidated in the ideal cleavage case (Griffith's criterion), it was soon understood that the same concept of crack toughness could be used in the more common situation where dissipative processes in the bulk of the solid (yet in the vicinity of the crack surface) contributes to (or even dominates over) the thermodynamic surface energy. A basic justification of this extension is that the additional dissipated energy is confined in a boundary layer within a small distance, δ, from the crack surface, the process zone. For large scale structures, as compared to δ, an *effective* surface energy — integrating all dissipative phenomena — is an operational concept.

In this up-scaling justification of the relevance of linear fracture mechanics, it should be emphasized that as the reference to a true surface energy is lost, so is the property that only the crack surface area matters. When a crack propagates in a heterogeneous solid, similarly, this heterogeneity may trigger different dissipative phenomena, resulting in a toughness which cannot be reduced to the bare surface energy. This effect have been exhibited in recent experimental studies [1–4] showing how periodic modulations of interface properties affect crack propagation. The modeling proposed by Tvergaard and Hutchinson [5] showed that the interplay of local plasticity and crack propagation could also produce such an effect.

Crack propagation and depinning transition - The effect of heterogeneities on crack propagation has been early discussed in the context of reinforcement by crack trapping with tough particles [6–8] and the detailed mechanism of overcoming a single obstacle has been clarified. This scenario leads to a local instability that can also be exploited to trigger dissipative (e.g. viscous) mechanisms that will result in an enhanced effective toughness. Although the individual mechanism can be very precisely modeled and described, the difficulty of considering crack propagation in a random heterogeneous medium is that "collective" pinning/depinning takes place and the wide distribution of avalanches (i.e. instabilities now involving potentially a large number of pinning sites) precludes a quantitative modeling of the effective toughness without using a detailed microscopic modeling.

Indeed, the advance of a planar crack front through a disordered medium can be seen as a dynamic phase transition [9–15]. The elastic energy release rate (or equivalently the stress intensity factor) plays here the role of a control parameter. Below threshold, the crack front only advances over a finite distance and eventually stops (static phase). Above threshold, the crack front cannot be arrested any longer and it reaches a finite velocity (mobile phase). The effective (macroscopic) toughness corresponds to the critical threshold. Beyond the field of crack propagation, the paradigm of the depinning transition [16] appears to describe as various physical phenomena as wetting of disordered interfaces, solid friction, plastic flow of crystalline or amorphous materials... The common characteristic feature of these different systems lies in the competition between the driving force, the pinning induced by a random potential at a microscopic scale and an elastic restoring force at large scale.

Depending on the relative strength of the random potential and elasticity of the front, one usually distinguishes two generic situations as illustrated in Fig.1:
- in weak disorder conditions, the depinning front is only slightly perturbed and smoothly advances as a whole, with modest velocity fluctuations. Viscous dissipation can indeed be turned to arbitrary low values in quasi-static conditions, and hence only the bare *average* surface energy will be relevant for the macroscopic toughness. Disorder plays only a role on the geometry of the crack front. A theoretical description of the crack front geometry can be described through a perturbation expansion

about the homogeneous case (see e.g. [17] for a recent review). Such an approach, in spite of the sophisticated theoretical treatment involved, cannot account for an enhanced toughening.
- in strong pinning conditions, the front advances intermittently, through a series of localized micro-instabilities, or "avalanches". During these unstable events, viscous dissipation is at play (even for quasi-static loading conditions) and finally contributes to the global energy balance as an enhanced effective toughness. A thorough discussion of the transition between weak pinning and strong pinning can for instance be found in [18].

It is therefore crucial to characterize and quantify the onset of strong pinning and to propose a way to evaluate toughness in this regime quantitatively without having to recourse to an exhaustive numerical modeling. Such is the purpose of the present study, which is based on a self-consistent approach that was proposed in [19, 20], but never tested quantitatively.

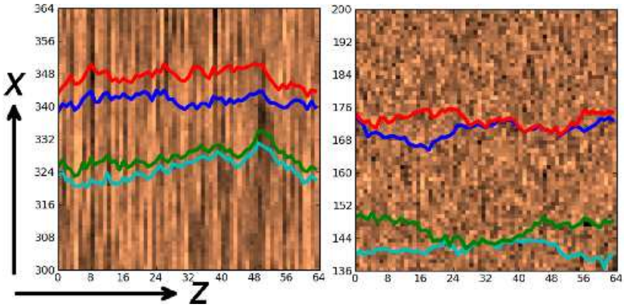

FIG. 1. Snapshots of crack fronts for different toughness landscape illustrating the transition from weak (left) to strong (right) pinning regimes – same distribution, different correlation lengths: $\xi_x = 16$ (left), $\xi_x = 1$ (right). Two sets of two fronts separated by a small time lag are represented. In weak pinning conditions (left), the distance between successive fronts is nearly constant, indicating that the local velocity only weakly fluctuates. In strong pinning conditions, parts of the front remain stuck while other ones have significantly advanced, indicating a jerky dynamics.

Numerical model - We consider here an interfacial crack front propagating in the (z, x) plane in $x-$direction. The location of the crack front at time t is denoted $h(z, t)$. A random toughness landscape $K_c(z, x)$ is considered. We denote its average $\overline{K_c}$ and its standard deviation S_c. In the following, the problem is made dimensionless by scaling stress intensity factors and toughness relative to $\overline{K_c}$. The reduced toughness (denoted as lowercase) $k_c(z, x) = K_c(z, x)/\overline{K_c}$ is now a random field of unit mean and standard deviation $\sigma = S_c/\overline{K_c}$. It is assumed to be short-range correlated and its correlation lengths are denoted ξ_x and ξ_z in the direction of propagation and orthogonal to it respectively.

The average stress intensity factor along the crack front, $K_0(t)$, i.e. the driving force, or its dimensionless counterpart $k_0(t) = K_0(t)/\overline{K_c}$, depends on both the macroscopic loading and problem geometry. We consider the classical case of a displacement controlled mechanical test driven at constant speed. To account for the stiffness of the system (specimen and loading device), the boundary condition is described by a slow and steady loading rate such that on average the crack front velocity is set to v_0. For this aim, we introduce the stiffness e such that

$$k_0(t) = e\left[v_0 t - \overline{h}(t)\right] \quad (1)$$

where $\overline{h}(t)$ is the average position of the front at time t.

The roughness of the crack front gives rise to a modulation of the local stress intensity factor. Using a first order expansion in the roughness [6] the dimensionless stress intensity factor at point $(z, x = h(z, t))$ can be written $k[z, h(z, t)] = k_0(t)\left[1 + k_{el}\left(z, h(z, t)\right)\right]$ where

$$k_{el}(z, h(z)) = \frac{1}{2\pi} ⨍ \frac{h(z) - h(z')}{(z - z')^2} dz' \quad (2)$$

(⨍ stands for the principal value of the integral).

Neglecting inertial effects, we consider in the following an over-damped dynamics and study the behavior of the crack front at the verge of propagation from above i.e. $v_0 \to 0^+$. In that framework, the front obeys the following equation of evolution:

$$\partial_t h(z, t) = \mathcal{R}\left[k_0(t) + k_{el}(z, h(z, t)) - k_c(z, h(z, t))\right] \quad (3)$$

where $\mathcal{R}$ denotes the positive part, $\mathcal{R}(x) \equiv \max(x, 0)$.

Note that the time scale has been set so that the viscosity is scaled to unity. Two parameters thus remain that characterize the driving dynamics: the (reduced) stiffness e and the (reduced) velocity v_0. In the following only the quasi-static limit $v_0 \to 0^+$ is considered. The random landscape of (reduced) toughness of unit mean is characterized by the standard deviation σ and the correlation lengths ξ_x and ξ_z. Note that, in the quasi-static limit, this simulation setup is expected to give the same results than extremal dynamics simulations [21].

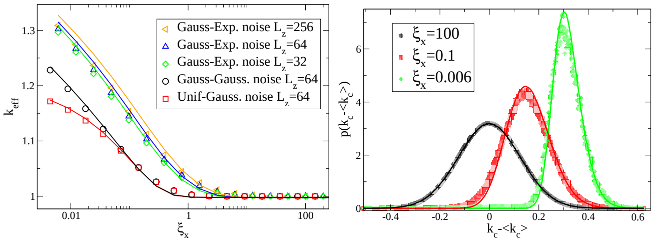

FIG. 2. Left: Effective toughness as a function of the correlation length ξ_x for different type of disorders and system widths L_z. Right: Toughness distribution along the crack front that propagates in an exponentially correlated Gaussian landscape of width $L_z = 64$ for different ξ_x, ($\sigma = 0.125$). Symbols and lines correspond to simulation data and theoretical predictions respectively.

In the following we generated random landscapes of sizes $L_z \times L_x$ with a unit lateral correlation length $\xi_z = 1$

(the discretization length scale in the lateral direction) and a tunable correlation length ξ_x in the direction of propagation. Three different types of random fields were considered: Uniform-Gaussian (UG), Gaussian-Gaussian (GG) and Gaussian-Exponential (GE) where the first term/letter refers to the probability distribution function of k_c and the second one qualifies its pair correlation function. The UG and GG disorders consist of grids of $N_z (= L_z/\xi_z) \times N_x (= L_x/\xi_x)$ random numbers from uniform and Gaussian distribution respectively. The space between grids points in the x direction follows a uniform distribution of mean ξ_x and standard deviation $\xi_x/2\sqrt{3}$. The generation of the GE landscape consists of realizations of an exponentially correlated Gaussian noise computed according to first order scheme due to Fox et al.[22] with an integration step $\Delta = \xi_x/50$. In all cases, the continuous toughness landscape $k_c(z, x)$ is interpolated linearly between two grid points in the x direction.

The standard deviation σ was varied in the range $[0.125 - 1]$ and the correlation length ξ_x in the range $[0.006 - 800]$. We used a reduced spring constant $e = 1$ and a reduced velocity $v_0 = \sigma/20$ (checked to be small enough not to influence significantly the results). Periodic boundary conditions along z are considered. Integration of Eq. 3 is performed according to an explicit mid-point scheme. The time step δt is chosen so that the maximum front increment is less than on tenth of the noise discretization size in the x direction. Starting from a flat configuration, we first integrate the crack front dynamic over a de-correlation length equal to $\xi_x(L_z/\xi_z)^{0.5}$ in order to reach a statistical steady state. The effective toughness k_{eff} is then computed as the mean value of the driving force minus the driving velocity $k_0 - v_0$ along a propagation length equal to $L_x = 1024\,\xi_x$. The effective toughness k_{eff} is finally averaged again over ten simulations (different statistical samples).

Numerical results - The weak-to-strong pinning transition induced by the shortening of the toughness correlation length has an important consequence: a spectacular increase of the effective toughness (the depinning threshold). Fig. 2(left) shows the dependence of the average value of the reduced stress intensity factor k_{eff} measured along the propagation of the front for different disorder types and the correlation length ξ_x of the anisotropic toughness landscape. For large values ξ_x we obtain $\langle k_{\text{eff}} \rangle \approx 1$ i.e. the mean of the toughness disorder $\langle k_c \rangle$. However for low values of ξ_x, we observe that k_{eff} departs from $\langle k_c \rangle = 1$ and can reach significantly higher values. We also note that the value of the effective toughness clearly depends on the type of distribution and correlation of the microscopic disorder. Such a dependence is certainly not surprising since the effective toughness is interpreted here as the threshold of a (dynamic) phase transition and as such is expected to depend on the microscopic details. We also note a slight but clear dependence on the system size: the larger the system, the larger the effective toughness. The enhancement of effective adherence is also reflected by changes in the toughness distribution (weighted by time) visited by the crack front as illustrated in Fig. 2. The full toughness distribution is clearly biased towards higher toughness values as ξ_x decreases.

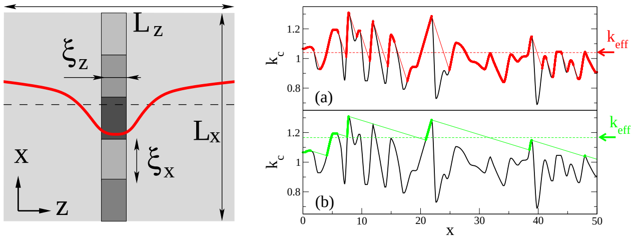

FIG. 3. Left: a band of random toughness in a homogeneous landscape traps the crack front; the lower the line stiffness, the larger the front deflection. Right: Graphical solutions of the implicit equation $\Delta k_{el}(x) = \Delta k_c(x)$ which determines the equilibrium position of the crack front. The stable positions in the band are highlighted (in red and green) for two values of the line stiffness. The slope of the fine lines between the stable portions corresponds to the stiffness S of the crack front (a) For large line stiffness, the trajectory corresponds almost to the toughness in the band (weak pinning). (b) For low stiffness, the equilibrium position toughness distribution is skewed toward higher toughness (strong pinning).

Interpretation: a self-consistent approach - This evolution can be rationalized in the framework of a self-consistent approximation proposed in Ref. [19] for illustration purpose, and never checked quantitatively. The top panel of Fig. 3 shows a toughness landscape consisting of a unique band of fluctuating toughness $k_c(x)$ in an otherwise homogeneous medium of toughness k_0. Because of the elastic coupling, the crack fronts undergoes a deflection $\Delta h = \overline{h} - h(0)$ proportional to the toughness contrast $\Delta k = k_c - k_0$. The associated line stiffness $S = \Delta k/\Delta h$ can be analytically computed from Rice formula[19, 23] and is shown to scale as $S \propto 1/\xi_z \log(L_z/\xi_z)$. An effective medium approximation, in the spirit of the self-consistent approximation, consists in evaluating k_{eff} as equal to the value of k_0 such that the average deflection of the front taken over the ensemble of successive *stable* positions of the front is zero.

From weak to strong pinning - The simplicity of the one dimensional picture of Fig. 3 allows one to define a criterion that determines the pinning regime. In absence of driving force, an equilibrium configuration of the front at position $h(z = 0, t) = x$ in the band is obtained when the elastic restoring force, $\Delta k_{el}(x) = S\Delta h(x)$, balances the toughness contrast $\Delta k_c(x)$. Depending on the respective amplitude of the line stiffness and the local toughness gradient, one can obtain for this implicit equation either a unique solution or multiple solutions for the front position x. A simple criterion for the transition from weak to strong pinning can thus be drawn from the onset of multistability. Under these conditions, strong pinning is obtained when

$$\frac{\sigma}{S\xi_x} > 1. \tag{4}$$

As schematically shown in Fig. 3(right) different sets of stable positions along the band are generated as a function of the line stiffness. For large $S\xi_x/\sigma$ the stable trajectory follows closely the toughness of the band as expected from the weak pinning regime. Conversely for lower $S\xi_x/\sigma$ the crack front will only visit a subset of high toughness values that characterize the strong pinning regime. As a consequence, the distribution of toughness at stable positions is skewed toward higher values.

Direct numerical integration of the effective medium model was performed in order to test quantitatively its reliability. S is first determined numerically to account for the discreteness of the simulated crack front. The reduced toughness distributions and their means are then generated from one dimensional trajectories as exemplified in Fig. 3(right). The comparison between the self-consistent approximation and the crack front simulations reported in Fig. 2 and in Fig. 4 shows a remarkable agreement. k_{eff} is very accurately reproduced as a function of ξ_x, L_z, σ and the different disorder types. Note that the model not only accounts for the effective toughness variations but also for the visited toughness distributions *without any free parameter*.

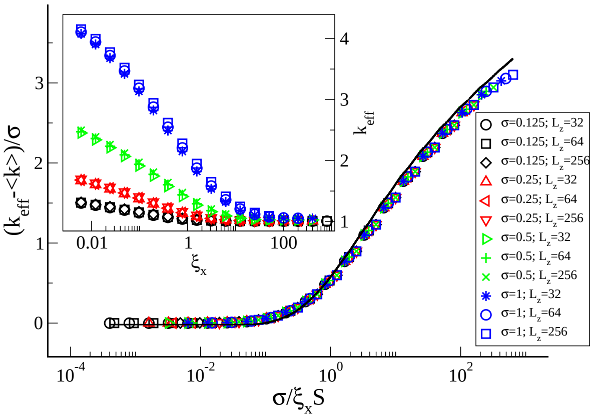

FIG. 4. Effective toughness as a function of the correlation length ξ_x for different toughness standard deviations σ and system widths L_z. The larger σ and/or the shorter ξ_x, the larger the effective toughness. Symbols and line correspond to simulation data and theoretical predictions respectively.

Scaling analysis - One can show that only a combination of scaled parameters really contributes to the observed results. If the toughness k, and distance x along the propagation direction, are transformed into

$$\begin{aligned} \tilde{k} &= (k - \langle k_c \rangle)/\sigma \\ \tilde{x} &= x/\xi_x \end{aligned} \tag{5}$$

then the elasticity of the crack front line is $\tilde{S} = S\xi_x/\sigma$. Note that $\tilde{k}$ has now a zero average and unit variance, and that the criterion for weak to strong pinning is simply $\tilde{S} = 1$. Fig. 4 shows the reduced effective toughness $\tilde{k}$ against the depinning control parameter $1/\tilde{S} = \sigma/S\xi_x$. All numerical estimates of effective toughness can be collapsed onto a single master curve that captures the transition. For small values of the control parameter $1/\tilde{S} \ll 1$ the weak pinning regime holds, $k_{\mathrm{eff}} = 1$, whereas, for large values $1/\tilde{S} \gg 1$, k_{eff} significantly increases (strong pinning). Note that the system size dependence is here captured in the line stiffness parameter (the latter increases as the logarithm of the crack front length). This has no effect in the weak-pinning regime, but introduces a rather counter-intuitive result in the framework of fracture mechanics: the larger the system, the smaller the line stiffness and hence the larger the effective toughness.

It thus appears that the disorder (local toughness pdf and spatial correlation) has a dramatic effect on the pinning conditions. A crack front can encounter weak or strong pinning depending on its propagation direction. In the same spirit, if the toughness landscape is non-symmetrical, the effective toughness in a given direction will not be the same as in the opposite one. Our approach thus offers a natural interpretation to the recent results presented in Ref. [3], but also a simple theoretical framework from which a detailed optimization can be carried out.

Conclusion - The depinning of a long-ranged elastic line appears to be strongly dependent on the spatial correlation of the disordered landscape through which it propagates. The transition between weak and strong pinning is well captured by a simple criterion build on the toughness gradient in the direction of propagation and the line stiffness. A simple self-consistent approximation describes very accurately the progressive departure of the depinning threshold from its weak pinning value (the mean value of the disorder) to the higher values measured in strong pinning conditions. In particular this approximation appears to accurately capture the dependence of the depinning threshold to the finer microscopic details (statistical distribution of toughness and spatial correlation function). Let us emphasize that such a result may not have been expected from the fact that strong pinning involves micro-instabilities and collective phenomena (avalanches, ...) due to the underlying dynamical phase transition.

Bearing in mind that the enhancement of the effective toughness does not originate from the initial landscape toughness distribution only but also from its spatial correlation, our results open a promising way to design anisotropic and tough interfaces. The present model gives also significant insights for safety calculation since it reproduces accurately the toughness distribution from which extreme statistics can be deduced. Finally, our approach offers interesting theoretical perspectives for other systems presenting the prototypical situation where elastic interface are trapped by random disorder.

S.P. acknowledges the support of ANR project MePhyStaR.

---

[1] D. A. Ramrus and J. C. Berg, Colloids and Surfaces A: Physicochemical and Engineering Aspects, **273**, 84 (2006), ISSN 0927-7757.

[2] R. Tadepalli, K. T. Turner, and C. V. Thompson, Acta Materialia, **56**, 438 (2008), ISSN 1359-6454.

[3] S. Xia, L. Ponson, G. Ravichandran, and K. Bhattacharya, Phys. Rev. Lett., **108**, 196101 (2012).

[4] L. Alzate, PhD dissertation (2012).

[5] V. Tvergaard and J. W. Hutchinson, Int. J. Solids Struct., **46**, 3433 (2009), ISSN 0020-7683.

[6] H. J. Gao and J. R. Rice, J. Appl. Mech., **56**, 828 (1989).

[7] A. F. Bower and M. Ortiz, J. Mech. and Phys. Solids, **39**, 815 (1991).

[8] T. M. Mower and A. S. Argon, Mechanics of Materials, **19**, 343 (1995).

[9] J. Schmittbuhl, S. Roux, J. P. Vilotte, and K. J. Måløy, Phys. Rev. Lett., **74**, 1787 (1995).

[10] P. Daguier, B. Nghiêm, E. Bouchaud, and F. Creuzet, Phys. Rev. Lett., **78**, 1062 (1997).

[11] S. Ramanathan and D. S. Fisher, Phys. Rev. Lett., **79**, 877 (1997); S. Ramanathan, D. Ertaş, and D. S. Fisher, *ibid.*, **79**, 873 (1997); S. Ramanathan and D. S. Fisher, Phys. Rev. B, **58**, 6026 (1998).

[12] A. Tanguy, M. Gounelle, and S. Roux, Phys. Rev. E, **58**, 15771590 (1998).

[13] D. Bonamy and E. Bouchaud, Physics Reports (2010).

[14] S. Santucci, K. Måløy, A. Delaplace, J. Mathiesen, A. Hansen, J. Ø. H. Bakke, J. Schmittbuhl, L. Vanel, and P. Ray, Phys. Rev. E, **75**, 016104 (2007).

[15] D. Dalmas, A. Lelarge, and D. Vandembroucq, Phys. Rev. Lett., **101**, 255501 (2008).

[16] M. Kardar, Phys. Rep., **301**, 85 (1998).

[17] V. Lazarus, J. Mech. Phys. Solids, **59**, 121 (2011).

[18] A. Tanguy and T. Vettorel, Eur. J. Phys. B, **38**, 71 (2004).

[19] S. Roux, D. Vandembroucq, and F. Hild, Eur. J. Mech. A, **22**, 743 (2003).

[20] S. Roux and F. Hild, Int. J. Fract., **154**, 159 (2008).

[21] D. Vandembroucq, R. Skoe, and S. Roux, Phys. Rev. E, **70**, 051101 (2004).

[22] R. F. Fox, I. R. Gatland, R. Roy, and G. Vemuri, Phys. Rev. A, **38**, 5938 (1988).

[23] J. Chopin, A. Boudaoud, and M. Adda-Bedia, Phys. Rev. Lett., **107**, 144301 (2011).